CrossMark

The effects of Cr and Si additions and deposition conditions on the structure and properties of the (Zr-Ti-Nb)N coatings

A.D. Pogrebnjak[a], A.A. Bagdasaryan[a,*], V.M. Beresnev[b], U.S. Nyemchenko[b], V.I. Ivashchenko[c], Ya.O. Kravchenko[a], ZH.K. Shaimardanov[d], S.V. Plotnikov[d], O. Maksakova[a]

[a] Sumy State University, 2, Rymsky Korsakov Str., 40007 Sumy, Ukraine
[b] Kharkiv National University, Svobody Sq., 4, 61022 Kharkiv, Ukraine
[c] Frantsevich Institute for Problems of Materials Science, National Academy of Sciences of Ukraine, str. Kryzhanovskogo 3, Kyiv 03680 Ukraine
[d] D. Serikbayev East Kazakhstan State Technical University, Ust-Kamenogorsk, Kazakhstan

ARTICLE INFO

ABSTRACT

In this study, (Zr-Ti-Nb)N, (Zr-Ti-Cr-Nb)N and (Zr-Ti-Cr-Nb-Si)N nitride coatings were obtained using a well-developed vacuum arc deposition. The systematical investigations demonstrate that the chemical composition, microstructure, and properties of the coatings intimately rely on the deposition parameters (pressure of working gas and substrate bias). Effects of Cr and Si additions on microstructure and mechanical properties of the (Zr-Ti-Nb)N coatings have been investigated using scanning electron microscopy (SEM) equipped with energy dispersive spectrum (EDS), X-ray photoelectron spectroscopy (XPS), X-ray diffraction (XRD), transmission electron microscope (TEM), hardness measurements and adhesion testing. First-principles band-structure calculations and Gibbs-Rosenbaum triangle representation have been used to investigate the elemental and phase compositions in nitride coatings. The multi-component (Zr-Ti-Cr-Nb-Si)N and (Zr-Ti-Nb)N coatings are found to be a simple face-centered cubic (FCC) solid solution. For the coatings without Si, the structure is mainly composed of TiN fcc phase and Cr_2N trigonal modification. The hardness values were in the ranges (24–42 GPa). The (Zr-Ti-Nb)N, (Zr-Ti-Cr-Nb)N coatings provided the best adhesive strength in different conditions. The (Zr-Ti-Cr-Nb-Si)N coatings exhibited the worst adhesive strength, which may be attributed to the relative low hardness.

1. Introduction

The development of nitride protective coatings roughly undergoes several different stages. The first is the classic strategy of alloying, which mainly have one principal element for the primary property requirement and the alloying additions for secondary properties (less than 5 at%) [1–4]. However, the disadvantages of these alloys are limits of the number of useful alloys that can be made. The second stage is the development of complex ternary and quaternary nitride coatings, having attracted significant research and industrial interest due to the unique combination of structural characteristics and exceptional mechanical properties [5–23].

In order to obtain the coatings with the strict requirements of high performances and functionalities high-entropy alloys (HEA's) have been proposed [24,25]. In a HEA system, there are five or more elements in equimolar ratio, and the concentration is between 5 and 35 at% for each element. It is well known, that the HEAs tend to form simple FCC- and/or BCC-type solid solution phases attributed to their

high mixing entropies. The high-entropy effects mean that the formation of disordered solid solutions is ensured by increasing of the contribution of configurational entropy to the mixing entropy due to the increasing of the constituent elements. According to the Boltzman's relation, with the increasing mixing entropy the free energy of mixing accepts the lowest values, which makes the solid solution more stable, especially at elevated temperatures. It should be noted that, the bulk high-entropy alloys have been investigated more intensive, in contrast to the coatings based on HEAs. There are only few studies on HEA coatings are available, such as: (TiZrNbHfTa)N [25], (AlCrMoTaTi)N [26], (AlCrNbSiTiV)N [27], (AlCrSiTiZr)N [28], (AlMoNbSiTaTiVZr)N [29] and (TiVNbZrHf)N [21]. The nitride films based on high-entropy alloys exhibit beneficial features and extraordinary properties, like excellent mechanical properties oxidation and wear resistance.

This study describes an initial attempt to analyze the phase stability of the nitride coatings with different number of constituent elements, which will lead to a deeper understanding of the complex relationship between microstructure and mechanical properties of multicomponent

Table 1
The deposition parameters of the (Zr-Ti-Nb)N, (Zr-Ti-Cr-Nb)N and (Zr-Ti-Cr-Nb-Si)N coatings.

№	Deposited Material	I_a, A	P_N, Pa	U, V
1	Zr-Ti-Nb	95	0.05	−100
2		95	0.5	−100
1	Zr-Ti-Cr-Nb	110	0.3	−100
2			0.7	−100
3			0.3	−200
4			0.7	−200
1	Zr-Ti-Cr-Nb-Si	110	0.3	−100
2		110	0.3	−200

Table 2
Elemental analysis of the (Zr-Ti-Nb)N, (Zr-Ti-Cr-Nb)N and (Zr-Ti-Cr-Nb-Si)N coatings.

Series №	Concentration, at%						
	Ti	Zr	Cr	Nb	N	Si	Impurity
(Zr-Ti-Nb)N							
1	20.91	20.38	–	19.99	39	–	–
2	20.52	19.36	–	19.26	41	–	–
(Zr-Ti-Cr-Nb)N							
1	10.21	6.63	15.22	4.96	62	–	0.57
2	12.30	8.48	16.92	6.17	56	–	–
3	11.27	8.03	18.23	7.48	55	–	–
4	10.40	7.81	11.00	6.73	64	–	0.39
(Zr-Ti-Cr-Nb-Si)N							
1	34.50	11.58	11.00	3.30	37	2.1	–
2	32.30	13.28	7.95	3.62	40	3.5	–

coatings. For this investigations five strong nitride forming elements Ti, Cr, Zr, Nb and V are selected for preparing protective nitride coatings by vacuum arc technique. The addition of silicon, which have partially solubility, will improve mechanical properties. It should be noted, that the binary nitrides like, TiN, CrN, ZrN, NbN and VN have FCC structure, whereas AlN, Si_3N_4 and BN: hexagonal or amorphous [30–37]. The formation of simple structure indicates that the non-FCC binary nitrides are dissolves into FCC nitrides. The presence of alloying elements in TiN-matrix, such as Cr, improves oxidation resistance, Zr contribute to better wear resistance, whereas Si and Nb increases the hardness and thermal stability.

In other words, the multielement solid solution containing elements from neighboring groups of different period, such as the Ti group (Ti, Zr), Nb and Cr results in a seriously distorted lattice because of the significant differences in the atomic size, which may significantly influence the structure and properties of these alloys.

This study focuses on the structural and mechanical properties of ternary and multicomponent (Zr-Ti-Nb)N, (Zr-Ti-Nb-Cr)N and (Zr-Ti-Nb-Cr-Si)N nitride coatings, obtained by vacuum arc deposition. The goal is to understand the influence of the small additions of Cr and Si elements and parameters of the deposition (negative substrate bias and working gas pressure) on the microstructure and properties of the films.

2. Experimental and computational details

2.1. Experiment procedures

The (Zr-Ti-Nb)N, (Zr-Ti-Cr-Nb)N and (Zr-Ti-Cr-Nb-Si)N coatings were deposited on polished rotating substrates (material – steel 12×18H9T, A 570 Grade 36 steel and Si) by vacuum arc deposition using a vacuum-arc device "Bulat −6″. The target alloys Zr-Ti-Nb (Zr – 35 at%, Nb – 35 at%, Ti – 30 at%), Zr-Ti-Cr-Nb (Cr – 37.39 at%, Zr – 27.99 at%, Nb – 22.30 at%, Ti – 12.32 at%) and Zr-Ti-Cr-Nb-Si (Cr –

17.08 at%, Zr – 30.19 at%, Nb – 9.67 at%, Ti – 39.96 at%, Si – 3.1 at%) were fabricated by electron-beam melting. The deposition of the (Zr-Ti-Nb)N, (Zr-Ti-Cr-Nb)N and (Zr-Ti-Cr-Nb-Si)N coatings were carried out in an N_2 atmosphere, the pressure of working gas changed from 0.05 to 0.7 Pa. The substrate bias was chosen as the controlling parameter, which varied from −100 to −200 V. The substrates were heated to 450 °C before deposition. The distance between the substrates and the cathode was 250 mm. The thickness of the (Zr-Ti-Nb)N and (Zr-Ti-Cr-Nb)N coatings were 4 and 6.2÷6.8 µm, respectively. The parameters of the deposition of the (Zr-Ti-Nb)N, (Zr-Ti-Cr-Nb)N and (Zr-Ti-Cr-Nb-Si)N coatings are presented in the Table 1.

The chemical compositions and morphology of the coatings were examined using X-ray energy-dispersive spectrometer system PEGASUS, scanning electron microscopy/energy-dispersive X-ray spectroscopy (SEM/EDX) JEOL JSM-6610 LV and JEOL 7001TTLS with a voltage of 15−20 kV.

The chemical bonding state of the films was analyzed by X-ray photoelectron spectroscopy (XPS, EC 2401, USSR) using MgK_α radiation (E=1253.6 eV). Prior to the XPS measurements, the samples were sputter-etched in argon plasma for 5 min

The crystal structure and phase composition were analyzed by X-ray diffraction (XRD) using D8 ADVANCE and DRON-4 diffractometers. The XRD patterns were taken in point-by-point scanning mode with a scanning step of 2θ=0.02…0.2° in the range of angles 25…90°. The direct studies of the structure of the (Zr-Ti-Cr-Nb)N coating was conducted using a JEOL JEM_2100 transmission electron microscope.

The study of the mechanical characteristics (hardness) of the nitride coatings was carried out on a DM-8 hardness tester. The imprints were
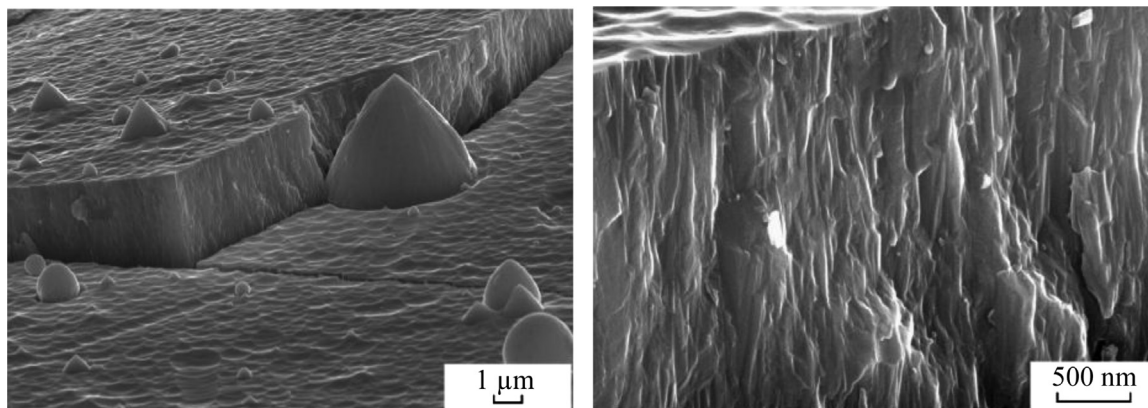
Fig. 1. Images of fracture patterns of (Ti-Zr-Nb)N coatings obtained at P_N=0,5 Pa.
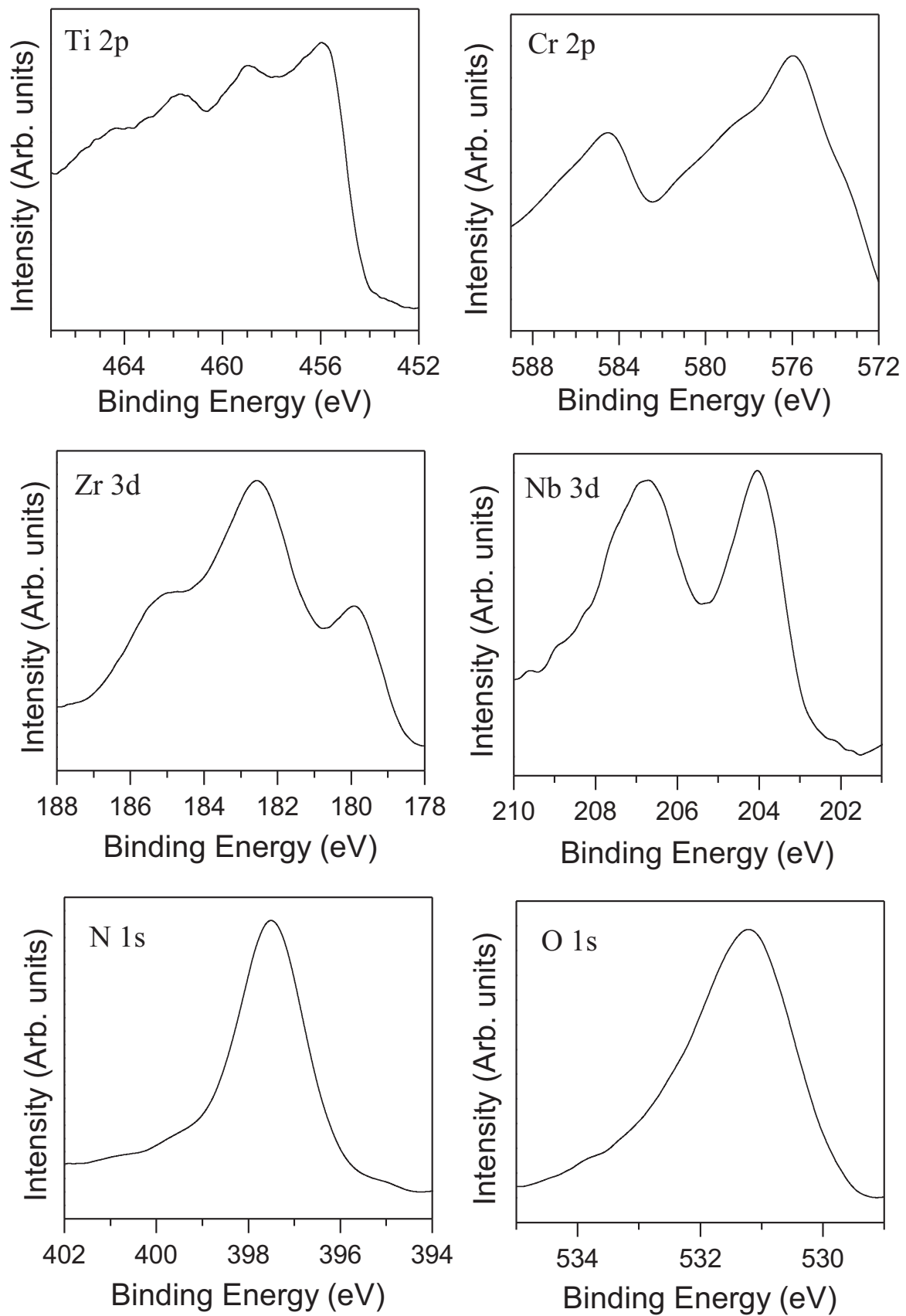
Fig. 2. XPS peaks of (Zr-Ti-Cr-Nb)N coating deposited at P_N=0,3 Pa and U=200 V.
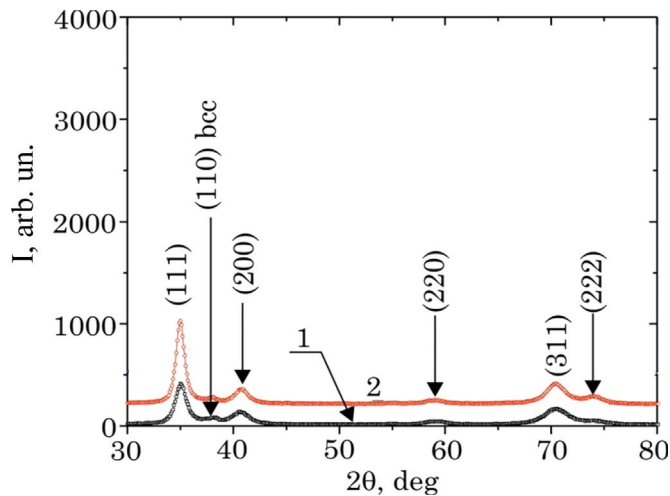
Fig. 3. Areas of the diffraction spectra of (Zr-Ti-Nb)N coatings obtained at different partial pressure of nitrogen: curve 1 – P_N=0.05 Pa; 2 – P_N=0.5 Pa.
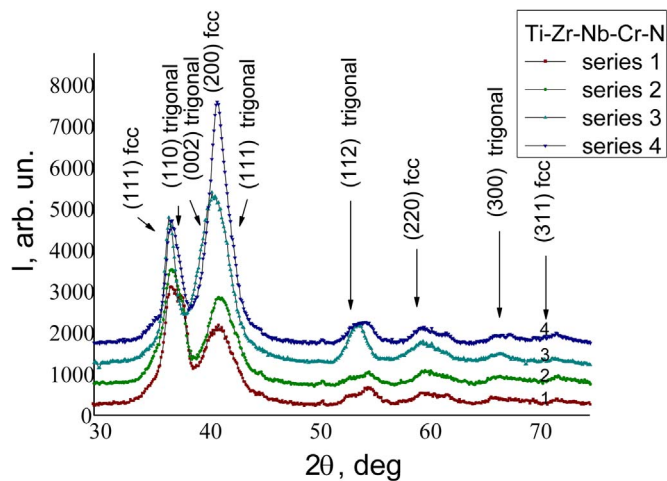

Fig. 4. XRD patterns of the (Zr-Ti-Cr-Nb)N nitride films deposited at different P_N and U values.

Table 3
Lattice constants and grain sizes of the (Zr-Ti-Cr-Nb-Si)N and (Zr-Ti-Cr-Nb)N nitride films estimated from XRD analysis.

№	Nitride coating	Lattice constant (nm)	Grain size (nm)
1	(Zr-Ti-Cr-Nb)N	0.4365	5.2
2		0.4359	4.5
3		0.4410	5.1
4		0.4381	6.9
1	(Zr-Ti-Cr-Nb-Si)N	0.4332	11.5
2		0.4337	9.7

made at a distance of 1.0 mm between each other, ten measurements were held for each sample. In order to reduce the impact of the droplet component, part of the coating had been polished after deposition.

Nanohardness and elasticity modulus were measured using nanoindentation (Hysitron TI 950 TriboIndenter) with Berkovich diamond indenter, maximal load was 10,000 μN. The values of hardness and elasticity modulus from load-unload curves using Oliver-Pharr method were measured.

A scratch tester REVETEST (CSM Instruments) equipped with a 200 mm tip radius Rockwell C diamond indenter was used to measure the adhesion of the (Zr-Ti-Nb)N, (Zr-Ti-Cr-Nb)N and (Zr-Ti-Cr-Nb-Si)N coatings. To obtain reliable results, two scratches on the surface of
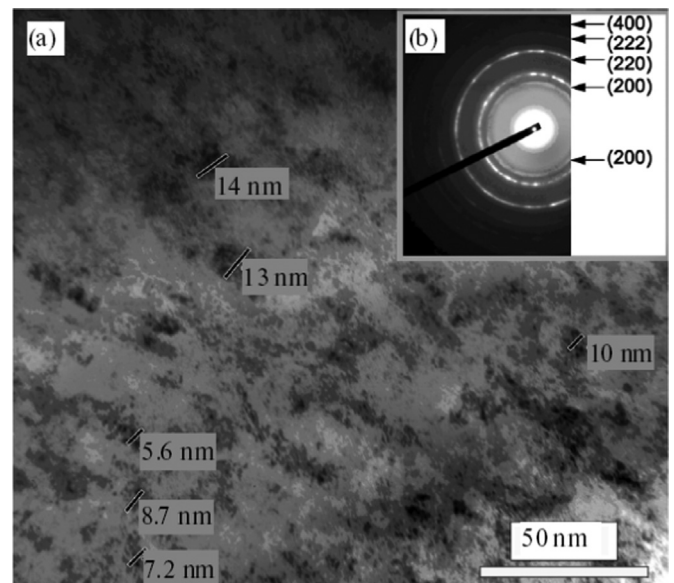

Fig. 5. Image of the (Zr-Ti-Cr-Nb)N coating produced using electron microscopy: bright field image (a), microdiffraction picture (b).
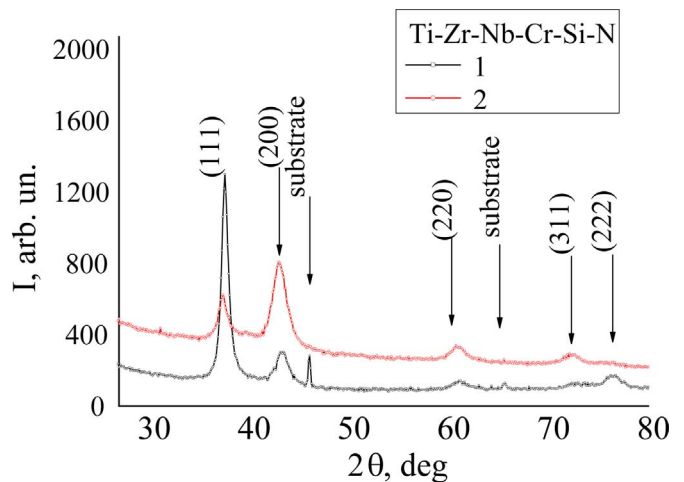

Fig. 6. XRD patterns of the (Zr-Ti-Cr-Nb-Si)N nitride films deposited at P_N=0.3 Pa and different U values (−100, −200 V).

Table 4
Mean values of hardness of the nitride coatings.

| Series	Hardness, GPa
(Zr-Ti-Nb)N HV$_{0.05}$ GPa	
1	37.2
2	44.5
(Zr-Ti-Cr-Nb)N HV$_{0.1}$ GPa	
1	30.9
2	34.7
3	38.8
4	43.9

the coating were made. The substrates for the deposition of the coatings were steel 18Cr10NiTi cylinders with a diameter of 30.0 mm and height of 5.0 mm. Used as a counterbody was a ball (Al$_2$O$_3$) with the diameter of 6.0 mm. The surface morphology of the friction track studied using scanning electron microscope FEI Nova NanoSEM 450.

The critical load responsible for the moment of appearance of the first chevron cracks at the bottom of the scratches was defined as L_{C1}; L_{C2} − the time of occurrence of chevron cracks at the bottom of the

Table 5
Comparative results of adhesion testing for the (Zr-Ti-Nb)N, (Zr-Ti-Cr-Nb)N and (Zr-Ti-Cr-Nb-Si)N coatings.

Critical loads (H)	Serial number			
	№1	№2	№3	№4
(Zr-Ti-Nb)N				
L_{C1}	2,91	9,89	–	–
L_{C2}	29,04	20,62	–	–
L_{C3}	43,18	36,43	–	–
L_{C4} (L_{C5})	59,26	66,77	–	–
(Zr-Ti-Cr-Nb)N				
L_{C1}	10,94	11,8	10,35	15,21
L_{C2}	18,69	20,93	18,42	24,29
L_{C3}	26,95	30,35	23,12	33,45
L_{C4}	39,15	45,94	45,12	40,97
L_{C5}	49,09	56,17	61,08	62,06
(Zr-Ti-Cr-Nb-Si)N				
L_{C1}	9,54	11,28	–	–
L_{C2}	12,48	14,04	–	–
L_{C3}	18,36	24	–	–
L_{C4}	29,86	34,09	–	–
L_{C5}	45,33	45,57	–	–
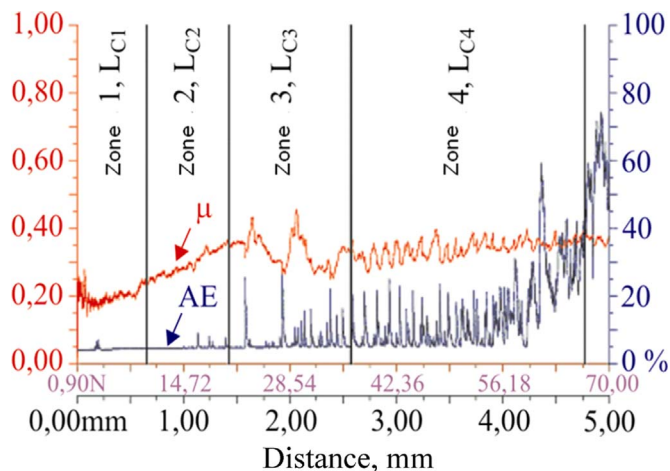
Fig. 7. Dependence of friction coefficient on the applied load at a scratch test of the coating (Ti-Zr-Nb)N, obtained at P_N=0.5 Pa.

scratches; L_{C3} – the destruction has cohesively-adhesive character; L_{C4} – local flaking of the areas of the coating; L_{C5} – plastic abrasion of the coating to the substrate, loss of adhesion strength.

2.2. Theoretical methods

First-principles band-structure calculations were carried out using the Quantum-ESPRESSO code [38] for 8-atom cubic supercells of $Ti_{4-n}Nb_nN_4$, $Ti_{4-n}Zr_nN_4$ and $Zr_{4-n}Nb_nN_4$, n=0, 1, 2, 3, 4, representing $Ti_{1-x}Nb_xN$, $Ti_{1-x}Zr_xN$ and $Zr_{1-x}Nb_xN$ alloys, respectively, with the B1 structure (space group Fm-3 m, No. 225). Vanderbilt ultra-soft pseudo-potentials were used to describe the electron-ion interaction [39]. The semi-core states were treated as valence states. To describe exchange-correlation energy, the generalized gradient approximation (GGA) of Perdew et al. [40] was employed. The criterion of convergence for the total energy was 10^{-6} Ry/formula unit. To speed up convergence, each eigenvalue was convoluted with a Gaussian with a width of 0.02 Ry. The cut-off energy for the plane-wave basis was set to 38 Ry. The integration in the Brillouin zone (BZ) was done on special **k**-points determined according to the Monkhorst-Pack scheme using a non-shifted mesh (8 8 8). All initial structures were optimized by simultaneously relaxing the supercell basis vectors and the atomic positions

inside the supercell using the Broyden-Fletcher-Goldfarb-Shanno (BFGS) algorithm [41]. The relaxation of the atomic coordinates and of the supercell was considered to be complete when atomic forces were less than 1.0 mRy/Bohr (25.7 meV/Å), stresses were smaller than 0.05 GPa, and the total energy during the structural optimization iterative process was changing by less than 0.1 mRy (1.36 meV).

To estimate the formation energies of the nitrides under consideration, the total energies of the Ti, Zr, Nb, Cr and Si crystal as well as the N_2 molecule were calculated. The structures based on Cr were considered in the paramagnetic state.

3. Results

Fig. 1 shows the images of surface coatings and fracture patterns of the (Zr-Ti-Nb)N coating. The study of surface morphology shows that the deposition of the coatings leads to increase the surface roughness (from 0.09 to 0.42 μm) due to the drop component of the plasma flow..

From the cross-sectional image in Fig. 1,b the coating showed the columnar structure, which is characterized for the materials obtained by vacuum arc deposition. It should be noted there are some micro voids and gaps among the columns.

The concentration of various elements in the (Zr-Ti-Nb)N, (Zr-Ti-Nb-Cr)N and (Zr-Ti-Nb-Cr-Si)N coatings under different parameters of deposition are listed in Table 2. The content of the elements in the all coatings was close to the concentration of elements in the sputtering target.

The chemical binding state and elemental composition of the (Zr-Ti-Cr-Nb)N coating were investigated by XPS (see Fig. 2) with peaks which associated with Ti 2p, Cr 2p, Zr 3d, Nb 3d, N 1 s. Also it was observed the oxygen (O 1 s) peak. According to the existing data [42] Ti 2p peaks at 455.8 and 458.7 eV are correspond to Ti-O and Ti-N bonds, respectively; Cr 2p peak at 576.1 eV to Cr-N bond; Zr 3d peaks at 180.1 eV and 182.2 eV to Zr-N and Zr-O bonds, respectively; Nb 3d at 203.8 eV and 207.5 eV to Nb-N and Nb-O bonds, respectively; N 1 s peak at 397.4 eV to Cr-N bond; O 1 s peak at 531.3 eV to Nb-O bonds. These results suggest that the (Zr-Ti-Cr-Nb)N coating is consist of Ti-N, Ti-O, Cr-N, Zr-N, Zr-O, Nb-N and NB-O bonds which could be attributed to TiN, TiO_2, Cr_2N, ZrN, ZrO_2, NbN and Nb_2O_5, respectively. Thus it can be assumed that the coatings formed multi-phase material (Ti, Zr, Nb)N-Cr..

Fig. 3 shows the XRD patterns of the (Zr-Ti-Nb)N nitride coatings. The analysis X-ray diffractometer spectrum shows that the determining phase composition is the phase with a face-centered cubic lattice. Low-intensity peak at 2θ =38° indicates the presence of small inclusions with BCC lattice, typical for vacuum-arc method for dropping phase (see Fig. 1, a). A characteristic feature with increasing pressure of the reaction gas (from 0.05 to 0.5 Pa) is strengthening the peaks of the family of planes {111}, which is determined by the increase of perfection preferred orientation of growth of crystallites with [111] axis perpendicular to the plane of the surface. It was found that the size of the crystallites increases from 10 nm at the lowest pressure of 0.05–63 nm at the maximum working pressure 0.5 Pa..

Phase analysis of (Zr-Ti-Cr-Nb)N nitride coatings indicates the presence of a TiN fcc phase (a=0.243 nm, a_{tab}=0.244 nm) and Cr_2N trigonal modification (P31m space group, a=0.4800 nm, c=0.4472 nm) (Fig. 4). From the XRD patterns, it is found that the substrate bias strongly influences the orientation changing from (111) preferred to (111) and (200) mixed and the appearance of the (112) and (300) reflections at high angles (Cr_2N trigonal phase). The structural analysis of the (Zr-Ti-Cr-Nb)N nitride coatings are in agreement with XPS results, whereas the coatings underwent phase segregation..

Table 3 lists the grain size and lattice parameters of the (Zr-Ti-Cr-Nb)N coatings, which were further evaluated from the XRD patterns. This table reveals that the lattice constant increases with increasing U. This is reasonable because the energetic bombardment causes incorporation of atoms of nitrogen into the spaces in the growing film that
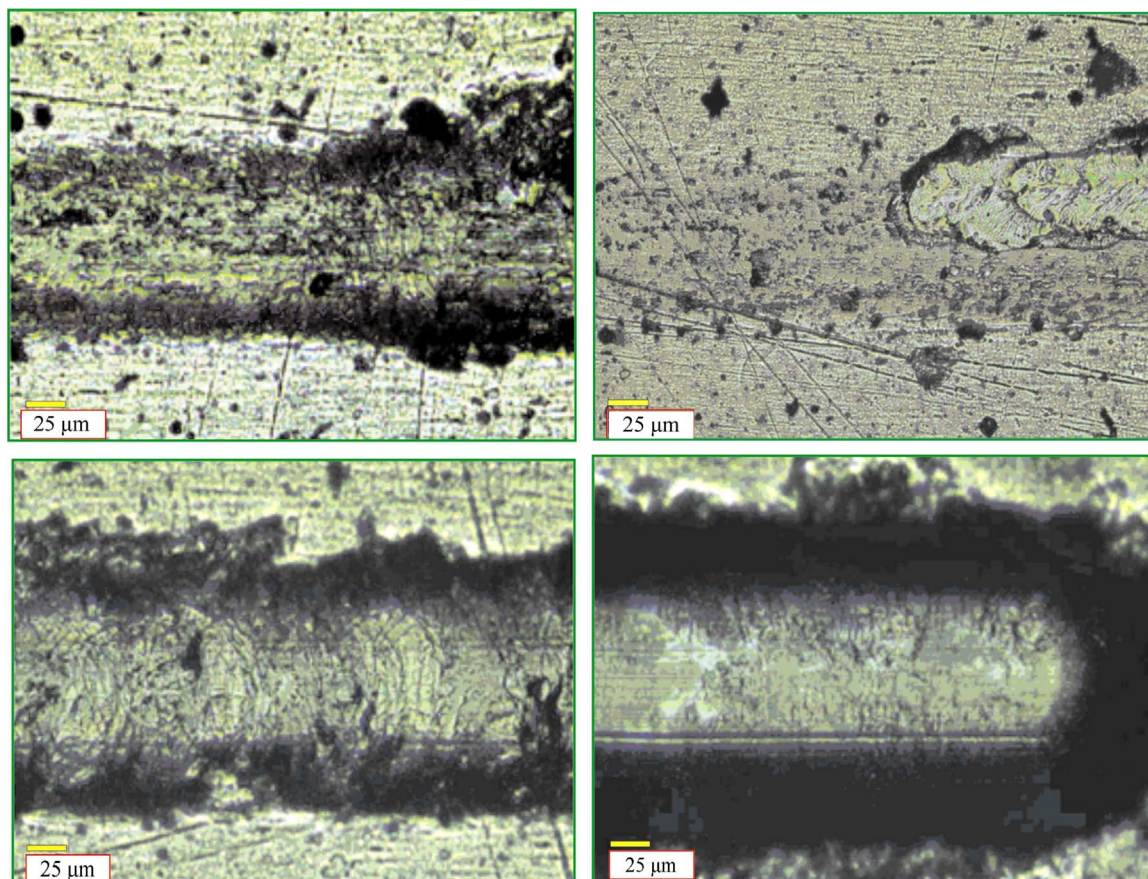
Fig. 8. Zones of contact of diamond indentor with the coating (Ti-Zr-Nb)N, obtained at P_N=0.5 Pa.
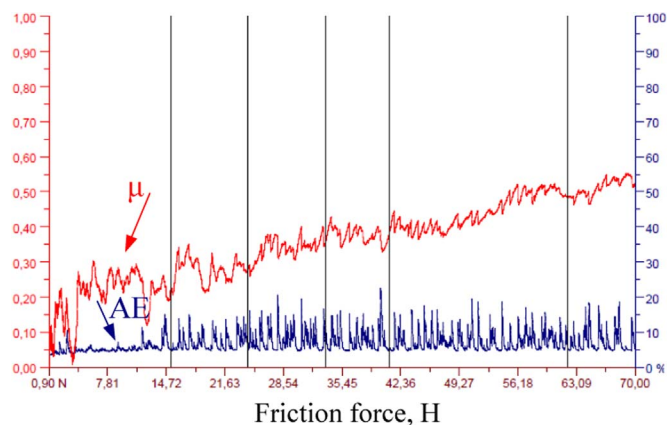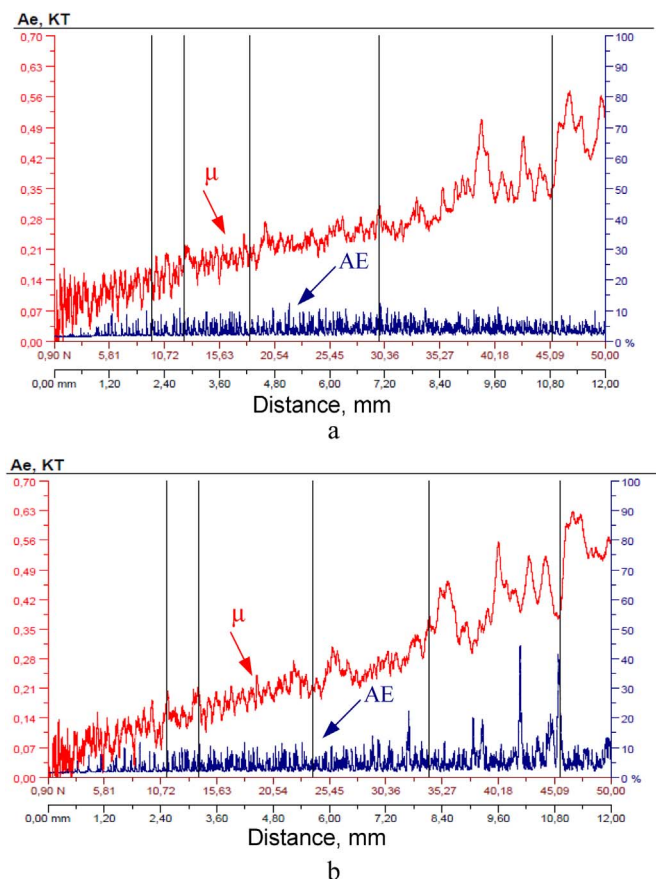

Fig. 9. The dependence of the friction coefficient and acoustic emission on the load on the specimen, coated with (Zr-Ti-Cr-Nb)N (series 4).

are smaller than the usual atomic volume ("atomic peening effect"). Additionally, the grain size of the (Zr-Ti-Cr-Nb)N nitride coatings is around 5.5 nm under all of the various potential biases, which means that the films possessed very fine nanocrystalline structures. This statement is confirmed by the results of electron microscopy and diffraction studies. As we can see from Fig. 5 transition metals of the Zr-Ti-Cr-Nb system during condensation form a coating with a fine-dispersed structure. In the electron-diffraction patterns, one observes rings of the fcc phase..

The XRD patterns of the (Zr-Ti-Nb-Cr-Si)N films deposited at P_N=0.3 Pa and U=100 and 200 V are shown in Fig. 6. As we can see the XRD patterns of the (Zr-Ti-Cr-Nb-Si)N coatings are greatly affected by the substrate bias. For nitride coatings, only XRD lines belonging to

(111), (200), (220), (222) and (311) peaks from the FCC structure of the B1 phase (NaCl-type) are evidenced. It is well known that nanocomposite coatings like TiSiN are characterized by the formation of amorphous (Si_3N_4)/crystalline (TiN) composite structures. The non-FCC nitride Si_3N_4 phase has low solubility in FCC structure, and thermodynamically driven (spinodal) segregation can occur during the deposition. It should be noted that the appropriate Si content to achieve the single layer (Si_3N_4) around each TiN grain is reported to be between 5–12 at%, although the exact amount varies depending on the average grain size [30–37]. In our case, even though the present systems contain several immiscible nitrides, for example TiN and Si_3N_4 (in small concentration), only a single FCC phase in the film was clearly identified (see Fig. 5). The formation of the FCC nitride phase has been related to the high mixing entropy effect and limited diffusion kinetics in which atoms cannot reach their stable configuration [43]..

It was found that with increasing substrate bias the positions of XRD peaks are shifted to lower angles (see Fig. 6). One of the explanations of this effect is the increase in the lattice parameters of the (Zr-Ti-Cr-Nb-Si)N coatings due to the formation of Frenkel pairs and anti-Schottky defects. This shift also can be explained by the fact that a small contraction of the NaCl type lattice with the presence of Si, perhaps due to a small incorporation of Si in the lattice and the formation of short Me-Si bonds. Furthermore, the increases concentration of Si probably causes the shift of the XRD peaks, indicating a possible changing of lattice constant [44,45]. The lattice parameters for the deposited (Zr-Ti-Cr-Nb-Si)N coatings increase gradually from 0.4332 nm at a negative substrate bias of 100–0.4337 nm at a bias of −200 V (see Table 3). The average grain sizes of the films was calculated from the XRD patterns using Scherrer's formula and were found to be strongly affected by the increase in the substrate bias. The crystallite size in the coating of series 1 (U to −100 V) averaged 11.5 nm, for the series 2−9.7 nm (U to −200 V). It is well known that

Fig. 10. The dependence of the friction coefficient and acoustic emission on the load on the specimen, coated with (Zr-Ti-Cr-Nb-Si)N: a – Series 1, b – Series 2.

the high-energy ion bombardment prevents the migration of grain boundaries due to the increasing the number of preferential nucleation sites, which decreases the grain size. As we can see from the results in Table 3, when the Si content increased from zero to 3.5 the crystallite size increased from 4.5 to 11.5 nm, whereas the lattice parameter decreased. Similar results have been obtained in different works devoted to the investigation of Si-containing nitride systems [44,45].

The results of measuring mechanical characteristics, in particular, hardness of the all obtained coatings, are shown in the Table 4. As seen from the Table 4, the maximal value of hardness (44.5 GPa) for the (Zr-Ti-Nb)N nitride coating is reached at the pressure of reaction gas P_N=0.5 Pa. As we can see, the hardness of the (Zr-Ti-Cr-Nb)N coatings deposited at P_N=0.3 Pa and U=−100 V are 30.9 GPa and change to 38.8 GPa as the substrate bias increases to −200 V. It should be noted that coatings deposited at lower nitrogen content exhibit low hardness. When the P_N increased to 0.7 Pa, the rise in hardness is explained by the formations of larger amounts of strong Me/N bonds present in the films. In addition, the high hardness may be due to the high content of Cr_2N phase, because the hardness of the Cr_2N coating is higher than CrN coating.

For the (Zr-Ti-Cr-Nb-Si)N nitride coatings, which deposited at P_N=0.3 Pa and U=−100 V, the hardness is 29 GPa and the elastic modulus is 291 GPa. With the increase of the potential bias to −200 V, the hardness and elastic modulus accordingly decreased to 24 and 254 GPa. One of the explanation of the decreasing hardness is excessive ion bombardment, resulting the coatings to become less textured, switching from a primarily (111) orientation with high intensity to contain FCC orientations including additional orientations of (111) and (200).

Table 5 shows the results of adhesion tests of the (Zr-Ti-Nb)N, (Zr-Ti-Cr-Nb-Si)N and (Zr-Ti-Cr-Nb)N coatings obtained at different

technological deposition parameters. The study results of the adhesive-cohesive strength, scratch resistance of the (Zr-Ti-Nb)N coatings shown on Fig. 7 and Fig. 8. Conventionally, the process of destruction of the coating in scratching with the indenter can be divided into four stages. At the load, range of 0.9−9.89 H (L_{C1}) appears the monotonically penetration of the indenter into the coating: the friction coefficient slightly increases the acoustic emission signal remains unchanged. When the load 15.81 H (L_{C2}) indenter is completely immersed in the coating. Slipping diamond indenter for cover run with friction coefficient 0.35. As the load increases 20.6−36.4 H (L_{C3}) occurs the extrusion of the material before the indenter as hillocks and increases the penetration depth of the indenter...

Comparative analysis demonstrates that the (Zr-Ti-Cr-Nb)N coatings are erased but not delaminated during scratching, i.e. destroyed by cohesive mechanism for plastic deformation and formation of the fatigue cracks in the coatings material. Fig. 9 show the curve of the change of the coefficient of friction (μ) when moving the diamond indenter on the surface of the coating of the (Zr-Ti-Cr-Nb)N system (sample 4), the curve of change of the acoustic emission (AE) and the image of the remaining fragmnts of the coating on the bottom of the scratch after the influence of the diamond indenter..

As we can see, monotonous penetration of the indenter into the coating takes place and the first cracks appear (load up to 15.21 N); the coefficient of friction (μ) is increasing, but the acoustic emission signal remains unchanged. Subsequently, with the increased load, the appearance of chevron and diagonal cracks takes place, which leads to the increase of the coefficient of friction to a value of 0.3. At a load of up to 14 N, the amplitude of the acoustic emission signal dramatically increases, and its value remains at the same level until the end of the test. After this, with the increase of the load reaching 62 N, there is local abrasion of the coating down to the substrate material.

The dependence of change in the coefficient of friction, acoustic emission and load on the specimen, coated with (Zr-Ti-Cr-Nb-Si)N, for Series 1 and Series 2 are shown in Fig. 10. As we can see, the loads of 9 N (L_{C1} for Series 1) and 11 N (L_{C1} for Series 2) correspond to the appearance of the first cracks and chips (see Figs. 11 and 12). This is confirmed by the beginning of the growth of the amplitude of the acoustic emission (Fig. 12). Initial abrasion of the coatings occurs under loads L_{C3}=18 N (Series 1) and L_{C3}=24 N (Series 2) (Figs. 11 and 12), which lead to the increase of the coefficient of friction to a value of 0.49 for all coatings. The local abrasion of the coatings down to the substrate material occurs when the load reaches values of 45 and 46 N. In this case, the friction coefficient increases to a maximum value of 0.63....

For (Zr-Ti-Cr-Nb-Si)N multicomponent coatings of Series 1, adhesion strength at different intervals of the experiment are significantly different from those of the samples of Series 2. With the increase of the load, noticeable crack propagation on the surface of the coating does not occur. Based on the nature of the destruction, the main contribution seems to be from the shear stresses. Cohesive failure occurs through cracking in the plane, perpendicular to the direction of growth of the coating. The first signs of abrasion for the coating were recorded under a load of 18 N.

Fig. 13 shows changes in the chemical composition of the (Zr-Ti-Cr-Nb-Si)N coatings during the scratch test. The dramatic increase the concentration of iron (distance 3 mm) corresponds to appearance of the first cracks and the beginning of the initial abrasion of the coatings. Furthermore, it should be noted that the content of iron increases more intensively in the coating, which obtained at U − 100 V. This statement is confirmed by the lower value of the critical load (18.36 and 24 H, respectively), which corresponds to the beginning of the initial abrasion of the coatings (see Table 5). The chemical compositions during the local abrasion of the (Zr-Ti-Cr-Nb-Si)N coatings is virtually the same, but the concentration of nitrogen in the Series 2 more higher, than in the Series 1, which is in agreement with EDX results. In addition, the concentration of Si and Nb elements remain constant during the
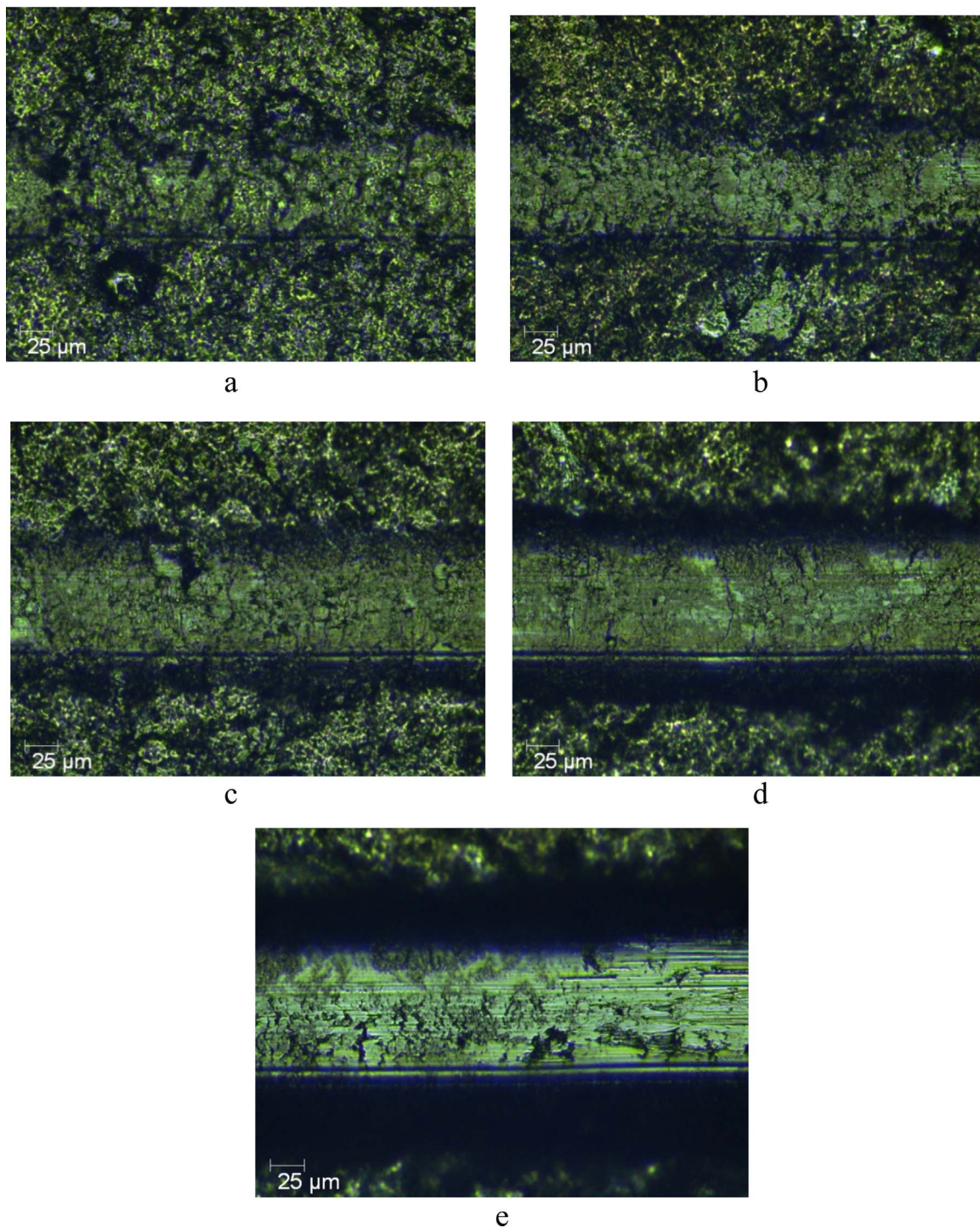
Fig. 11. Photos of the scratches on the samples of coatings of Series 1 (Zr-Ti-Cr-Nb-Si)N under different loads on the indenter: a − 9,54 H (L_{C1}); b − 12,48 H (L_{C2}); c − 18,36 H (L_{C3}); d − 29,86 H (L_{C4}); e − 45,33 H (L_{C5}).

scratch test for all coatings..

4. Discussion

4.1. Growth mechanism of nitride coatings

From XRD analysis, shown in Figs. 3, 4 and 6, it is found that all of the (Zr-Ti-Nb)N and (Zr-Ti-Cr-Nb-Si)N coatings formed a single solid solution nitride phase rather than separate nitrides coexisting with one another. Though several factors, such as non-equilibrium process of physical vapor deposition, high entropy of mixing (for multicomponent coatings) and a slight difference in the atomic radii, might contribute to the formation of crystal structures. These results also show that the as-deposited nitrides, such as $Zr_xTi_{1-x}N$, $Cr_xTi_{1-x}N$, $Nb_xTi_{1-x}N$, (AlCrTaTiZr)N, (CrTaTiVZr)N, (TiHfVNbZr)N [46–48].

In Fig. 14 we show the Gibbs free energy of mixing of the alloys under investigation, calculated at T=0 K (i.e., formation energy) as a function of composition x. The positive formation energy implies that the $Ti_{1-x}Zr_xN$ alloys are not stable, and will decompose into TiN and ZrN with the chemical driving force (E_{mix}). However, all alloys can be stabilized in some range of composition, depending on temperature, since the configurational entropy is always positive and promotes a
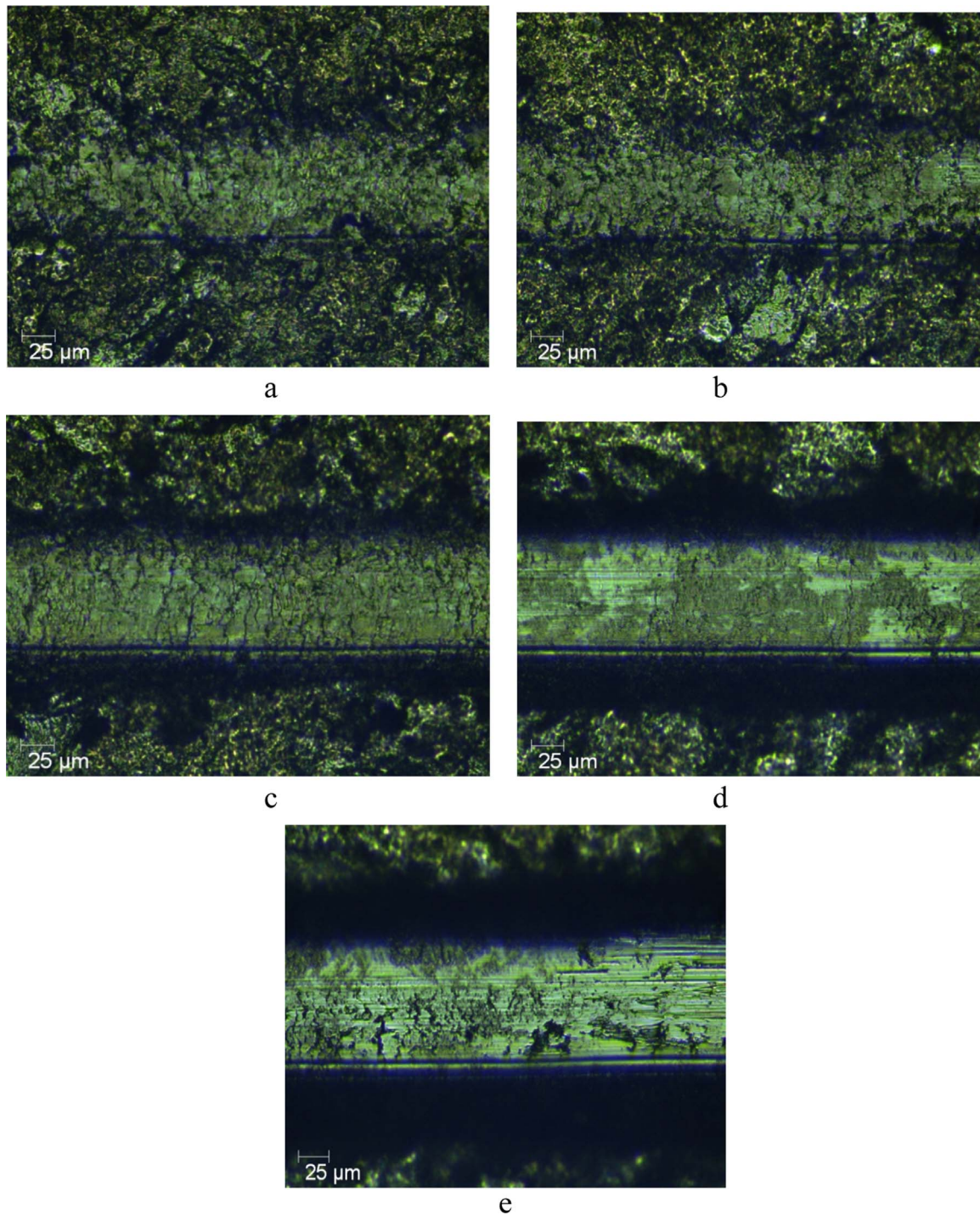
Fig. 12. Photos of the scratches on the samples of coatings of Series 2 (Zr-Ti-Cr-Nb-Si)N under different loads on the indenter: a − 11,28 H (L_{C1}); b − 14,04 H (L_{C2}); c − 24 H (L_{C3}); d − 34,09 H (L_{C4}); e − 45,57 H (L_{C5}).

decrease in Gibbs free energy. Since the values of E_{mix} for $Ti_{1-x}Nb_xN$ and $Zr_{1-x}Nb_xN$ are very small and some of them are negative, these alloys can be stabilized as solid solutions at moderate temperatures. These findings confirm the possibility of the formation of FCC solid solutions based on TiN, ZrN and NbN in thin films. Since in our films we observed only solid solutions based on these nitrides, one can suppose that the presence of NbN in the films precludes the separation of TiN and ZrN from the $Ti_{1-x}Zr_xN$ alloys..

However, for the (Zr-Ti-Cr-Nb)N coatings the experimental results point to the existence of two-phase structure: TiN fcc phase (a=0.243 nm, a_{tab}=0.244 nm) and Cr_2N trigonal modification (P31m

space group, a=0.4800 nm, c=0.4472 nm). The formation of a two-phase structure is obviously related to the presence of high concentrations of Cr and Nb elements, which have a low enthalpy of formation of nitrides (see Table 6). Cecchini et al. [49] indicated that with the increasing nitrogen pressure the crystalline phase of the coatings shift from Cr_2N (main phase)+CrN to CrN (main phase)+Cr_2N. These results are confirmed by Gibbs-Rosenbaum triangle representation (see Fig. 15). The vertices of an equilateral triangle correspond to a content of 100% of each system component. The method of defining the elemental composition based on the fact, that the sum of perpendiculars from any point within an equilateral triangle on each side is
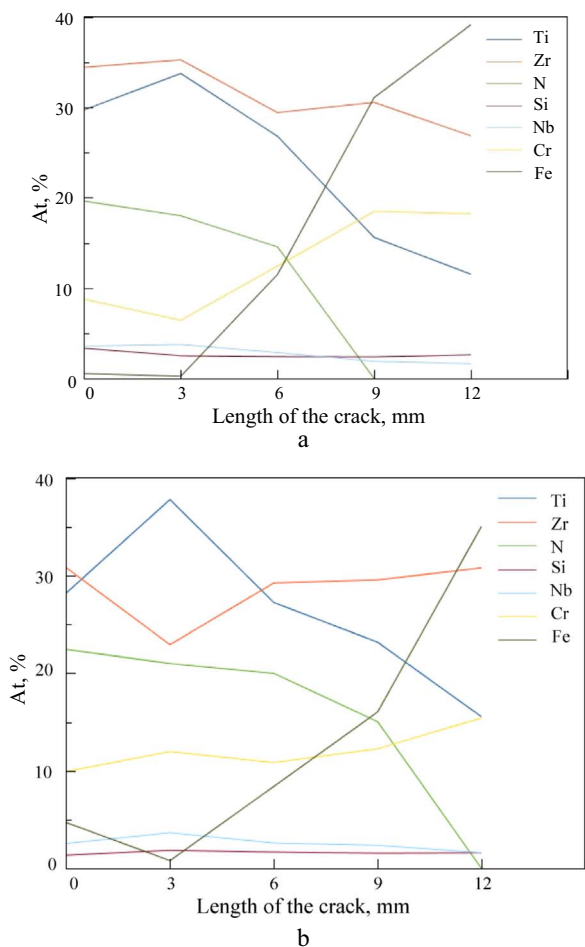
Fig. 13. Chemical composition of the coatings scratches after test: a – Series 1; b – Series 2.

Fig. 14. Computed mixing energy (E_{mix}) of $Ti_{1-x}Nb_xN$, $Ti_{1-x}Zr_xN$ and $Zr_{1-x}Nb_xN$ alloys as a function of composition x.

Table 6
The enthalpy of formation of nitrides of constituent elements of investigated nitride coatings.

	TiN	ZrN	NbN	CrN	Cr_2N	Si_3N_4
ΔH, kJ/mole	−337.7	−365.3	−234.7	−117.2	−129	−106

equal to the height of the triangle. Rosenbaum suggested using the three segments of straight lines parallel to the sides of the triangle and extending from this point to the intersection with each of the sides of the triangle. The sum of three line segments for each point within an equilateral triangle is equal to the length of its sides. As you can see from Fig. 15 that percentage content of the Ti-N, Zr-N systems is higher than of the Cr-N and Nb-N, thus it leads to forming of solid solution with high content of TiN and ZrN..

It is well known that the application of substrate bias potential can significantly change the film structures and their properties. When a substrate bias is applied, the reactive gas and metallic ions bombard the substrate. With the increase of substrate bias, the energetic ion bombardment becomes more intense. Because of an enhanced bombardment effect the coating densification is increased by decreasing the voided regions in the microstructure.

It should be noted that, a (111) preferred orientation was observed in the all coatings with a substrate bias U=−100 V. When the substrate bias was increased to U=−200 V, the nitride films presented a strong (200) and relatively weak (111) orientation. This phenomenon may be due to different kinetic constraints (anisotropy in surface diffusivities, adatom mobilities and collisional cascade effects) which are assumed to affect the preferential orientation [50–52].

4.2. Tribological properties of nitride films deposited under different parameters deposition

The test results of the adhesion strength show that the coatings were worn during scratching, but did not peel off, i.e. the destruction
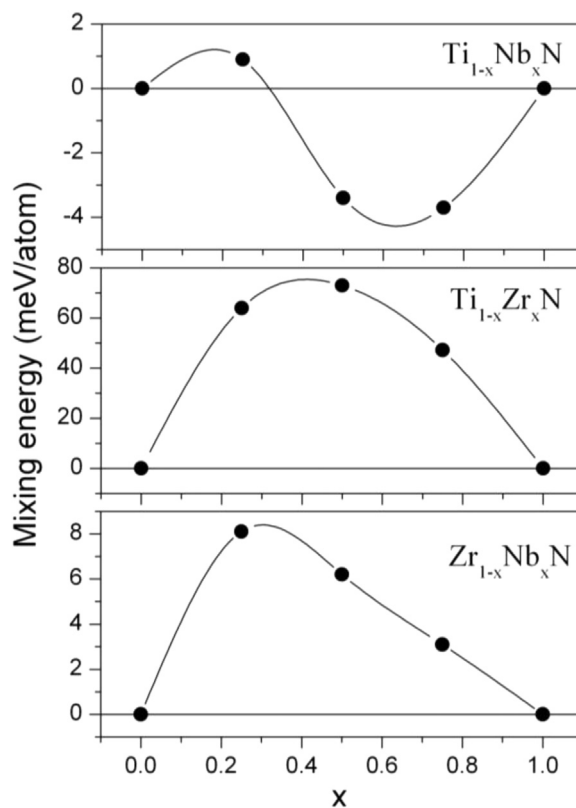
occurs by cohesive mechanism, associated with the plastic deformation and formation of fatigue cracks in the material of the coating.

Comparative analysis demonstrates (see Table 5), that the difference in the adhesion strength of the coatings seems to be caused by the differences in their structure and mechanical properties.

As shown in Table 5, with increasing the substrate bias, the adhesion strength between coatings and substrate is increase. The enhanced adhesion may be attributed to an enhanced resistance of crack formation and plastic deformation. The loads (L_{C5}) for the (Zr-Ti-Cr-Nb)N and (Zr-Ti-Cr-Nb-Si)N coatings increase with increasing substrate bias (from −100 to −200 V) their maxima of 62.06 and 45.57 N, respectively. In addition, it should be noted, that coatings, obtained under high bias, possessing the higher hardness are more resistant [53–57]. Nitride coatings (Zr-Ti-Cr-Nb)N and (Zr-Ti-Cr-Nb-Si)N with good adhesion strength demonstrate high values of hardness, 43.9 and 27.5 GPa, respectively. Comparing the results from Tables 4, 5 we can see that the coatings with high hardness possess good adhesive strength.

It has been reported that the application of substrate bias during the initial growth may cause collisional intermixing and thus an improvement of adhesion [58,59]. We believe that the additional reason for improved adhesion strength is an intermixing near the coating/substrate interface.
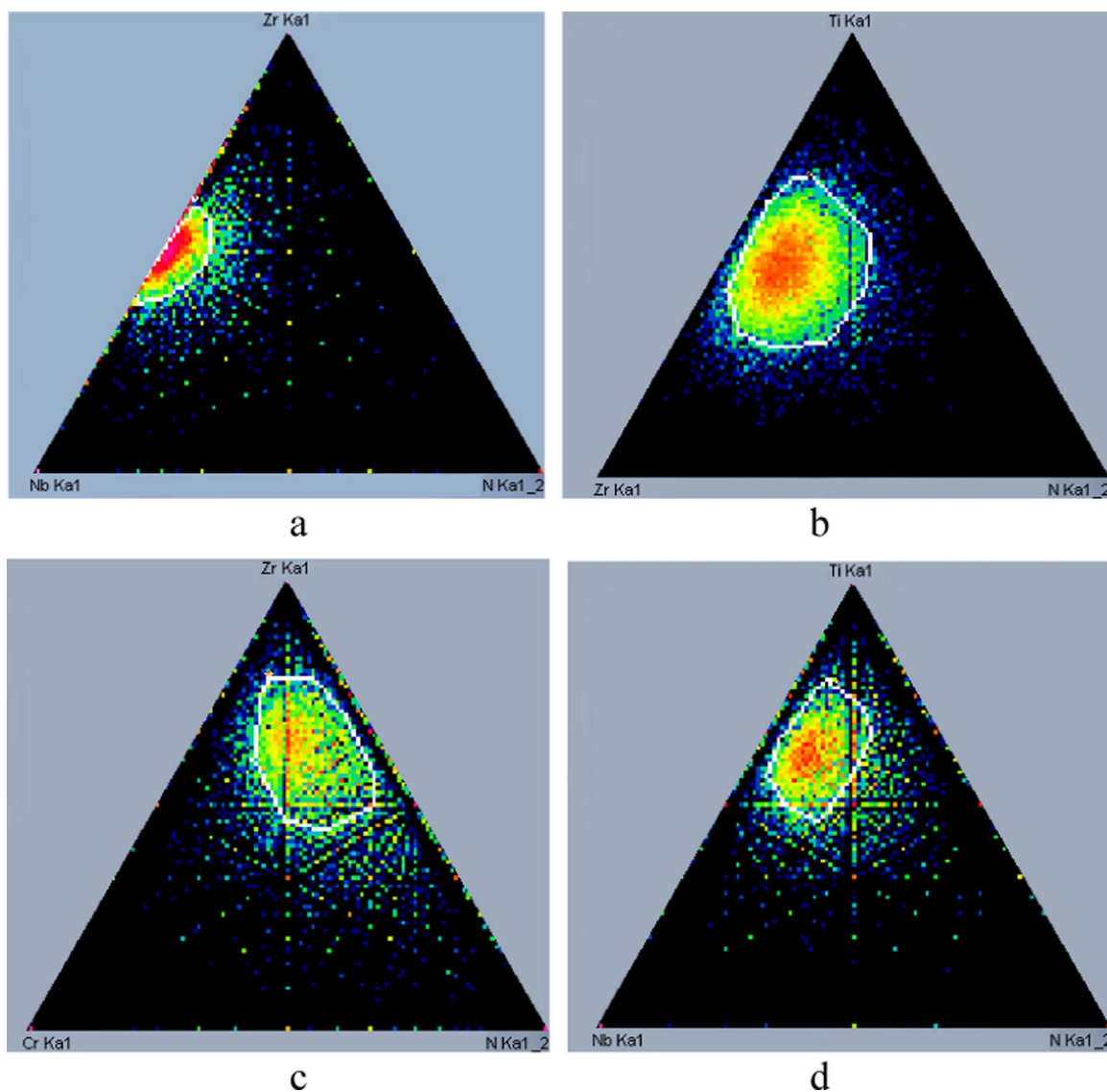
Fig. 15. Triangle map of elemental distribution, obtained from EDS: a) in the Nb-Zr-N solid solution; b) Zr-Ti-N solid solution; c) Cr-Zr-N solid solution; d) Nv-Ti-N solid solution.

5. Conclusion

The role of Cr and Si additions on the properties of (Zr-Ti-Nb)N coatings, including structure, relative hardness and adhesion had been investigated. The results of the study were summarized as followed:

– The ternary nitride coatings possess a FCC solid-solution nanocrystalline structure, with an (111) texture. The additions of Si element contribute to the formation the single solid solution with FCC structure; for the coating without Si additions, the structure is mainly composed of a TiN fcc phase and Cr_2N trigonal modification, which is obviously related to the presence of high concentrations of the elements with low enthalpy of formation of nitrides. No peak related with nitrides of silicon was detected.
– All coatings were determined to have nano-grained structures with grain sizes in the range of 5.2 and 63 nm.
– The (Zr-Ti-Nb)N, (Zr-Ti-Cr-Nb)N and (Zr-Ti-Cr-Nb-Si)N coatings have harnesses in the range of 37–45 GPa, 31–42 GPa and 24-29 respectively. The enhancement in the hardness of the coatings was attributed to the formation of the preferred orientation of the growth of crystallites with the [111] axis.
– It was found that the adhesion of investigated coatings was improved by applying the higher parameters of deposition (substrate bias and pressure of nitrogen). The local abrasion of the (Zr-Ti-Cr-Nb-Si)N coatings down to the substrate material occurs when the load reaches highest value of 46 N, for (Zr-Ti-Cr-Nb)N coatings – 62 N and for (Zr-Ti-Nb)N – 66 N.

References

[1] J.H. Sundgren, H.T.G. Hentzell, A review of the present state of art in hard coatings grown from the vapor phase, J. Vac. Sci. Technol. A 4 (1986) 2259–2279.
[2] I. Petrov, P.B. Barna, L. Hultman, J.E. Greene, Microstructural evolution during film growth, J. Vac. Sci. Technol. A 21 (2003) 117–128.
[3] S. Tan, X. Zhang, X. Wu, F. Fang, J. Jiang, Effect of substrate bias and temperature on magnetron sputtered CrSiN films, Appl. Surf. Sci. 257 (2011) 1850–1853.
[4] H.O. Pierson, Handbook of Refractory Carbides and Nitrides, Noyes, New Jersey, 1996.
[5] J.L. Endrino, S. Palacin, M.H. Aguirre, Determination of the local environment of

silicon and the microstructure of quaternary CrAl(Si)N films, Acta Mater. 55 (2007) 2129–2135.

[6] P. Zukowski, T.N. Koltunowicz, V. Bondariev, A.K. Fedotov, J.A. Fedotova, Determining the percolation threshold for $(FeCoZr)_x(CaF_2)_{(100-x)}$ nanocomposites produced by pure argon ion-beam sputtering, J. Alloy Compd. 683 (2016) 62–66.

[7] D.D. Kumar, N. Kumar, S. Kalaiselvam, S. Dash, R. Jayavel, Substrate effect on wear resistant transition metal nitride hard coatings: microstructure and tribo-mechanical properties, Ceram. Int. 41 (2015) 9849–9861.

[8] P. Zukowski, T.N. Koltunowicz, O. Boiko, V. Bondariev, K. Czarnacka, J.A. Fedotova, A.K. Fedotov, I.A. Svito, Impedance model of metal-dielectric nanocomposites produced by ion-beam sputtering in vacuum and its experimental verification for thin films of $(FeCoZr)_x(PZT)_{(100-x)}$, Vacuum 120 (2015) 37–43.

[9] D.C. Tsai, Z.C. Chang, B.H. Kuo, Y.C. Liu, E.C. Chen, F.S. Shieu, Structural, electro-optical, and mechanical properties of reactively sputtered (TiZrHf)N coatings, Ceram. Int. 42 (2016) 14257–14265.

[10] T.N. Koltunowicz, P. Zukowski, V. Bondariev, J.A. Fedotova, A.K. Fedotov, The effect of annealing on the impedance of $(FeCoZr)_x(CaF_2)_{(100-x)}$ nanocomposite films produced by the ion-beam sputtering in vacuum, Vacuum 120 (2015) 44–50.

[11] M.W. Kim, H.S. Tak, M.C. Kang, K.H. Kim, I.D. Park, T.J. Je, Cutting performance of nanocomposite Cr-C-N, Cr-Si-N and Cr-Si-C-N coated tools for micro end-milling operation, Curr. Appl. Phys. 9 (2009) e201–e204.

[12] J.H. Park, W.S. Chung, Y.R. Cho, K.H. Kim, Synthesis and mechanical properties of Cr-Si-N coatings deposited by a hybrid system of arc ion plating and sputtering techniques, Surf. Coat. Technol. 188–189 (2004) 425–430.

[13] C.S. Sandu, R. Sanjinés, M. Benkahoul, F. Medjani, F. Lévy, Formation of composite ternary nitride thin films by magnetron sputtering codeposition, Surf. Coat. Technol. 14 (2006) 4083–4089.

[14] A.K. Fedotov, V. Shepelevich, S. Poznyak, L. Tsybulskaya, A. Mazanik, I. Svito, S. Gusakova, P. Zukowski, T.N. Koltunowicz, Simulation of polycrystalline bismuth films Seebeck coefficient based on experimental texture identification, Mater.Chem. Phys. 177 (2016) 813–195.

[15] J.L. Ruan, D.F. Lii, J.S. Chen, J.L. Huang, Investigation of substrate bias effects on the reactively sputtered ZrN diffusion barrier films, Ceram. Int. 35 (2009) 1999–2005.

[16] A.D. Pogrebnjak, A.P. Shpak, G.V. Kirik, N.K. Erdybaeva, M.V. Il'yashenko, A.A. Dem'yanenko, Yu.A. Kunitskii, A. Sh Kaverina, V.S. Baidak, N.A. Makhmudov, P.V. Zukowski, F.F. Komarov, V.M. Beresnev, Sh.M. Ruzimov, A.P. Shypylenko, Multilayered nano-microcomposite Ti-Al-N/TiN/Al2O3 coatings. Their structure and properties, Acta Phys. Pol. A 120 (1) (2011) 94–99.

[17] A.D. Pogrebnjak, O.V. Sobol', V.M. Beresnev, P.V. Turbin, S.N. Dub, G.V. Kirik, A.E. Dmitrenko, Features of the structural state and mechanical properties of ZrN and Zr(Ti)-Si-N coatings obtained by ion-plasma deposition technique, Tech. Phys. Let. 35 (10) (2009) 925–928.

[18] O.V. Sobol, A.D. Pogrebnjak, V.M. Beresnev, Effect of the preparation conditions on the phase composition, structure, and mechanical characteristics of vacuum-Arc Zr-Ti-Si-N coatings, Phys. Met. Metallogr. 112 (2011) 188–195.

[19] A.D. Pogrebnjak, A.G. Ponomarev, D.A. Kolesnikov, V.M. Beresnev, F.F. Komarov, S.S. Mel'nik, M.V. Kaverin, Effect of mass transfer and segregation on the formation of superhard nanostructured Ti-Hf-N(Fe) coatings, Tech. Phys. Lett. 38 (2012) 623–626.

[20] A.D. Pogrebnjak, A.P. Shpak, V.M. Beresnev, M.V. Il'yashenko, F.F. Komarov, A.P. Shypylenko, M.V. Kaverin, P.V. Zukovski, Y.A. Kunitskyi, D.A. Kolesnikov, O.V. Kolisnichenko, N.A. Makhmudov, Structure and properties of nano- and microcomposite coating based on Ti-Si-N/WC-Co-Cr, Acta Phys. Pol. A 120 (2011) 100–104.

[21] A.D. Pogrebnjak, I.V. Yakushchenko, A.A. Bagdasaryan, O.V. Bondar, R. Krause-Rehberg, G. Abadias, P. Chartier, K. Oyoshi, Y. Takeda, V.M. Beresnev, O.V. Sobol, Microstructure, physical and chemical properties of nanostructured (Ti-Hf-Zr-V-Nb)N coatings under different deposition conditions, Mater.Chem. Phys. 147 (2014) 1079–1091.

[22] A.D. Pogrebnjak, B.A. Postol'nyi, Y.A. Kravchenko, A.P. Shipilenko, O.V. Sobol', V.M. Beresnev, A.P. Kuz'menko, Structure and Properties of (Zr-Ti-Cr-Nb)N Multielement Superhard Coatings, J. Superhard Mater. 37 (2015) 101–111.

[23] J.W. Yeh, S.K. Chen, S.J. Lin, J.Y. Gan, T.S. Chin, T.T. Shun, Nanostructured high-entropy alloys with multiple principal elements: novel alloy design concepts and outcomes, Adv. Eng. Mater. 6 (2004) 299–303.

[24] A.D. Pogrebnjak, A.A. Bagdasaryan, I.V. Yakushchenko, V.M. Beresnev, The structure and properties of high-entropy alloys and nitride coatings based on them, Rus.Chem. Rev. 83 (11) (2014) 1027–1061.

[25] V. Braic, M. Balaceanu, M. Braic, A. Vladescu, S. Panseri, A. Russo, Characterization of multi-principal-element (TiZrNbHfTa)N and (TiZrNbHfTa)C coatings for biomedical applications, J. Mech. Behav. Biomed. Mater. 10 (2012) 197–205.

[26] D.C. Tsai, Z.C. Chang, B.H. Kuo, M.H. Shiao, S.Y. Chang, F.S. Shieu, Structural morphology and characterization of (AlCrMoTaTi)N coating deposited via magnetron sputtering, Appl. Surf. Sci. 282 (2013) 789–797.

[27] P.K. Huang, J.W. Yeh, Effects of nitrogen content on structure and mechanical properties of multi-element (AlCrNbSiTiV)N coating, Surf. Coat. Technol. 203 (2009) 1891–1896.

[28] H.T. Hsueh, W.J. Shen, M.H. Tsai, J.W. Yeh, Effect of nitrogen content and substrate bias in mechanical and corrosion properties of high-entropy films $(AlCrSiTiZr)_{100-x}N_x$, Surf. Coat. Technol. 206 (2012) 4106–4112.

[29] M.H. Tsai, C.W. Wang, C.H. Lai, J.W. Yeh, J.Y. Gan, Thermally stable amorphous $(AlMoNbSiTaTiVZr)_{50}N_{50}$ nitride films diffusion barrier in copper metallization, Appl. Phys. Let. 92 (2008) (052129(1)–052129(3)..

[30] P.J. Martin, A. Bendavid, J.M. Cairney, M. Hoffman, Nanocomposite Ti-Si-N, Zr-Si-N, Ti-Al-Si-N, Ti-Al-V-Si-N thin film coatings deposited by vacuum arc deposi-

[31] N. Jiang, Y.G. Shen, H.J. Zhang, S.N. Bao, X.Y. Hou, Superhard nanocomposite Ti-Al-Si-N films deposited by reactive unbalanced magnetron sputtering, Mater. Sci. Eng. B 135 (2006) 1–9.

[32] D. Philippon, V. Godinho, P.M. Nagy, Endurance of TiAlSiN coatings: effect of Si and bias on wear and adhesion, Wear 270 (2011) 541–549.

[33] S. Veprek, M.G.J. Veprek-Heijman, The formation and role of interfaces in superhard nc-MeN/aSi$_3$N$_4$ nanocomposites, Surf. Coat. Technol. 201 (2007) 6064–6070.

[34] Y.H. Cheng, T. Browne, B. Heckerman, P. Gannon, J.C. Jiang, E.I. Meletis, C. Bowman, V. Gorokhovsky, Influence of Si content on the structure and internal stress of the nanocomposite TiSiN coatings deposited by large area filtered arc deposition, J. Phys. D. Appl. Phys. 42 (2009) 125415.

[35] Y.H. Cheng, T. Browne, B. Heckerman, E.I. Meletis, Mechanical and tribological properties of nanocomposite TiSiN coatings, Surf. Coat. Technol. 204 (2010) 2123–2129.

[36] J. Prochazka, P. Karvankova, M.G.J. Veprek-Heijman, S. Veprek, Conditions required for achieving superhardness of ≥45 GPa in nc-TiN/a-Si$_3$N$_4$ nanocomposites, Mater. Sci. Eng. A 384 (2004) 102–116.

[37] M.H. Hsieh, M.H. Tsai, W.J. Shen, J.W. Yeh, Structure and properties of two Al-Cr-Nb-Si-Ti high-entropy nitride coatings, Surf. Coat. Technol. 221 (2013) 118–123.

[38] P. Giannozzi, S. Baroni, N. Bonini, M. Calandra, R. Car, C. Cavazzoni, D. Ceresoli, G.L. Chiarotti, M. Cococcioni, I. Dabo, A. Dal Corso, S. de Gironcoli, S. Fabris, G. Fratesi, R. Gebauer, U. Gerstmann, C. Gougoussis, A. Kokalj, M. Lazzeri, L. Martin-Samos, N. Marzari, F. Mauri, R. Mazzarello, S. Paolini, A. Pasquarello, L. Paulatto, C. Sbraccia, S. Scandolo, G. Sclauzero, A.P. Seitsonen, A. Smogunov, P. Umari, R.M. Wentzcovitch, QUANTUM ESPRESSO: a modular and open-source software project for quantum simulations of materials, J. Phys.: Cond. Mat. 21 (2009) 395502–395519.

[39] D. Vanderbilt, Soft self-consistent pseudopotentials in a generalized eigenvalue formalism, Phys. Rev. B 41 (1990) 7892–7895.

[40] J.P. Perdew, K. Burke, M. Ernzerhof, Generalized Gradient Approximation Made Simple, Phys. Rev. Lett. 77 (1996) 3865–3868.

[41] S.R. Billeter, A. Curioni, W. Andreoni, Efficient linear scaling geometry optimization and transition-state search for direct wavefunction optimization schemes in density functional theory using a plane-wave basis, Comput. Mater. Sci. 27 (2003) 437–445.

[42] C.D. Wagner, Handbook of XPS, Physical Electronics Inc., Minnesota, 1995.

[43] H. Holleck, Metastable coatings – Prediction of composition and structure, Surf. Coat. Technol. 36 (1988) 151–159.

[44] H. Kim, S.R. Choi, S.Y. Yoon, Superhard Ti-Si-N coatings by a hybrid system of arc ion plating and sputtering techniques, Surf. Coat. Technol. 161 (2002) 243–248.

[45] D. Pilloud, J.F. Pierson, A.P. Marques, A. Cavaleiro, Structural changes in Zr-Si-N films vs. their silicon content, Surf. Coat. Technol. 180 (2004) 352–356.

[46] C.H. Lai, S.J. Lin, J.W. Yeh, S.Y. Chang, Preparation and characterization of AlCrTaTiZr multi-element nitride coatings, Surf. Coat. Technol. 201 (2006) 3275–3280.

[47] Z.C. Chang, D.C. Tsai, E.C. Chen, Structure and characteristics of reactive magnetron sputtered (CrTaTiVZr)N coatings, Mater. Sci. Semicond. Proc. 39 (2015) 30–39.

[48] A.A. Bagdasaryan, E. Smirnova, P. Konarski, M. Misnik, A. Zawada, The analysis of elemental composition and depth profiles of nitride nanostructures coating based on the TiHfVNbZr high-entropy alloy, JNEP 6 (2014) 02028(1)–02028(5).

[49] R. Cecchini, A. Fabrizi, M. Cabibbo, C. Paternoster, B.N. Mavrin, V.N. Denisov, N.N. Novikova, M. Haidopoulo, Mechanical, microstructural and oxidation properties of reactively sputtered thin Cr/N coatings on steel, Thin Solid Films 519 (2011) 6515–6521.

[50] G. Abadias, Stress and preferred orientation in nitride-based PVD coatings, Surf. Coat. Technol. 202 (2008) 2223–2235.

[51] L. Petrov, J.E. Hultman, J.E. Sundgen, Green, Polycrystalline TiN films deposited by reactive bias magnetron sputtering: effects of ion bombardment on resputtering rates, film composition, and microstructure, J. Vac. Sci. Tech. A10 (1992) 265–272.

[52] D. Gall, S. Kodambaka, M.A. Wall, I. Petrov, J.E. Greene, Pathways of atomistic processes on TiN(001) and (111) surfaces during film growth: an ab initio study, J. Appl. Phys. 93 (2003) 9086–9094.

[53] A.D. Pogrebnjak, I.V. Yakushchenko, O.V. Bondar, V.M. Beresnev, K. Oyoshi, O.M. Ivasishin, H. Amekura, Y. Takeda, M. Opielak, C. Kozak, Irradiation resistance, microstructure and mechanical properties of nanostructured (TiZrHfVNbTa)N coatings, J. Alloy Compd. 679 (2016) 155–163.

[54] A.D. Pogrebnjak, O.V. Bondar, G. Abadias, V. Ivashchenko, O.V. Sobol, S. Jurga, E. Coy, Structural and mechanical properties of NbN and Nb-Si-N films: experiment and molecular dynamics simulations, Ceram. Int. 42 (2016) 11743–11756.

[55] W. Liu, A. Li, H. Wu, R. He, J. Huang, Y. Long, X. Deng, Q. Wang, C. Wang, S. Wu, Effect of bias voltage on microstructure, mechanical properties, and wear mechanism of novel quaternary (Ti, Al, Zr)N coating on the surface of silicon nitride ceramic cutting tool, Ceram. Int. 42 (2016) 17693–17697.

[56] A. Shypylenko, A.V. Pshyk, B. Grzeskowiak, K. Medjanik, B. Peplinska, K. Oyoshi, A. Pogrebnjak, S. Jurga, E. Coy, Effect of ion implantation on the physical and mechanical properties of Ti-Si-N multifunctional coatings for biomedical applications, Mater. Des. 110 (2016) 821–829.

[57] A.A. Goncharov, Mechanism of formation of the columnar structure in films of transition metal diborides, Phys. Solid State 50 (2008) 168–172.

[58] K. Yamamoto, T. Sato, K. Takahara, K. Hanaguri, Properties of (Ti,Cr,Al)N coatings with high Al content deposited by new plasma enhanced arc-cathode, Surf. Coat. Technol. 174 (2003) 620–626.

[59] P. Hones, R. Sanjine, F. Levy, Sputter deposited chromium nitride based ternary compounds for hard coatings, Thin Solid Films 332 (1998) 240–246.

The effects of Cr and Si additions and deposition conditions on the structure and properties of the (Zr-Ti-Nb)N coatings [Текст] / A.D. Pogrebnjak, A.A. Bagdasaryan, V.M. Beresnev [та ін.] // Ceramics International. — 2017. — №43(1). — p. 771-782.